FULL PAPER

Advanced Charged Sponge-Like Membrane with Ultrahigh Stability and Selectivity for Vanadium Flow Batteries

Yuyue Zhao, Mingrun Li, Zhizhang Yuan, Xianfeng Li, Huamin Zhang,* and Ivo F. J. Vankelecom*

Advanced charged sponge-like porous membranes with ultrahigh stability and selectivity are designed and fabricated for vanadium flow battery (VFB) applications. The designed porous membranes are fabricated via constructing positively charged cross-linked networks on the pore walls of polysulfone membranes. The charge density of the pore walls can be tuned by changing the crosslinking time. The positively charged pore walls can effectively retain vanadium ions via Donnan exclusion, hence keeping extremely high selectivity, while the crosslinked network effectively increases the membrane stability. As a result, the designed membranes exhibit an outstanding performance, combining extremely high selectivity and stability. The single cell assembled with the prepared porous membrane shows a columbic efficiency of 99% and an energy efficiency of 86% at a current density of 80 mA cm^{-2}, which is much higher than Nafion 115 (93.5%; 82.3%). A battery assembled with the prepared membrane shows a stable battery performance over more than 6000 cycles, which is by far the longest record for porous membranes ever reported. These results indicate that advanced, charged, sponge-like, porous membranes with a crosslinked pore-wall structure are highly promising for VFB applications.

1. Introduction

Over the last few years, intense attention has been paid on large-scale energy storage due to its urgent need in grid management, load leveling and peak shaving, backup power, utilization and integration of renewable energy sources.[1,2] A vanadium flow battery (VFB) with the attractive features of independently tunable power and capacity, long cycle life, high safety, high efficiency and environmental friendliness has become one of the most promising technologies for large-scale energy storage.[2,3] Significant progress has been achieved in VFB technology over the past few decades, which is currently at demonstration stage.[2,4] Even though the availability and the merits of a VFB in different application fields have been well confirmed, the commercial progress of VFB has so far been hindered by the high cost (500–700 dollar m^{-2}) and low selectivity of perfluorinated membranes (Nafion).[5–7] Therefore, an urgent need still exists in developing high-performance membranes to assemble an acceptable VFB system.[7] Various nonperflourinate membranes,[8] such as sulfonated or quaternized aromatic polymer membranes, have been well studied on account of their attractive features like high selectivity, tunable ion conductivity, and low cost. However, the required properties are hardly satisfied by any of the current non-perflourinate membranes due to their low chemical stability, which was proven to be induced by the ion-exchange groups.[9] To address this challenge, porous membranes with transport based on the pore size exclusion mechanism, had been proposed and employed in VFB.[10] Different from traditional ion-exchange membranes, these porous membranes could selectively transfer ions, while excluding vanadium ions by combined pore size exclusion and Donnan exclusion. Based on this idea, different porous membranes based on polyacrylonitrile (PAN),[10,11] poly(vinylidene fluoride) (PVDF)[12] and poly(ether sulfone) (PES)[13] have been designed and fabricated. Afterwards, different modifications based on structure design and membrane assembly have been carried out to further improve membrane performance. For example, positively charged sponge-like porous membranes were fabricated by introducing pyridine groups in the pore walls for VFB application.[14] The advanced design could perfectly combine

Y. Zhao, Z. Yuan, Prof. X. Li, Prof. H. Zhang
Division of Energy Storage
Dalian Institute of Chemical Physics
Chinese Academy of Sciences
Zhongshan Road 457, Dalian 116023, P. R. China
E-mail: lixianfeng@dicp.ac.cn; zhanghm@dicp.ac.cn
Y. Zhao, Z. Yuan
University of Chinese Academy of Sciences
Beijing 100039, P. R. China
Prof. M. Li
State Key Laboratory of Catalysis
Dalian Institute of Chemical Physics
Chinese Academy of Sciences
Dalian 116023, P. R. China
Prof. X. Li, Prof. H. Zhang
Collaborative Innovation Centre of Chemistry for Energy Materials (iChEM)
Dalian 116023, P. R. China
Prof. I. F. J. Vankelecom
Centre for Surface Chemistry and Catalysis
Faculty of Bioscience Engineering
Katholieke Universiteit Leuven (KU Leuven)
Kasteelpark Arenberg 23 – Box 2461, B-3001 Leuven, Belgium

DOI: 10.1002/adfm.201503390

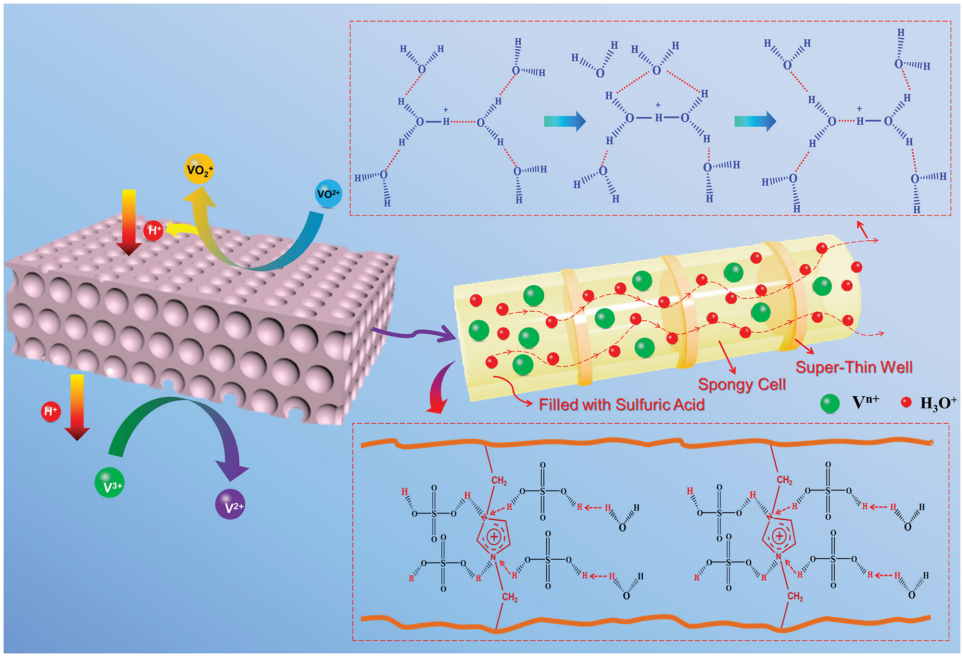

Scheme 1. Principle of the advanced charged sponge-like membrane with an internal crosslinked network applied in a VFB.

high selectivity and high conductivity, showing much better performance than Nafion 115. However, the stability of these membranes needs to be further improved to meet practical applications. Therefore, to explore porous membranes for practical application, combining high efficiency and high stability is one of the most important remaining challenges. Extensive efforts have thus been dedicated to improve the chemical stability of membranes, among which crosslinking[15] is proven to be one of the most efficient ways to improve the hydrolytic and oxidative stability of the membranes. For example, Zhang et al.[16] fabricated a blend anion-exchange membrane based on PSF and PVDF via a dictation cross-linking strategy for VFB application. The VFB assembled with the prepared membrane exhibited a CE of 99% and an EE of 84% at a current density of 80 mA cm^{-2}, while it kept a stable performance after running for more than 900 cycles. Our recent work proved that introducing internal crosslinking networks[17] would dramatically improve the stability of anion-exchange membranes as well, even though the introduction of ion-exchange groups would still affect membrane stability.

A new kind of advanced porous membrane with super-high stability and selectivity is now proposed (**Scheme 1**). The designed membrane combines the advantages of anion-exchange membranes and porous membranes, where positively charged imidazole groups were introduced on the pore walls of sponge-like PES porous membranes. In this design, the ion conductivity is assured by selective "ion diffusion" through the pore size exclusion and via the typical "Grotthuss mechanism" from "anion-exchanged groups." The imidazole could react with chloromethylated polysulfone (CMPSF) to form an internal crosslinking network on the pore wall, ensuring excellent selectivity and chemical stability of the membranes. The

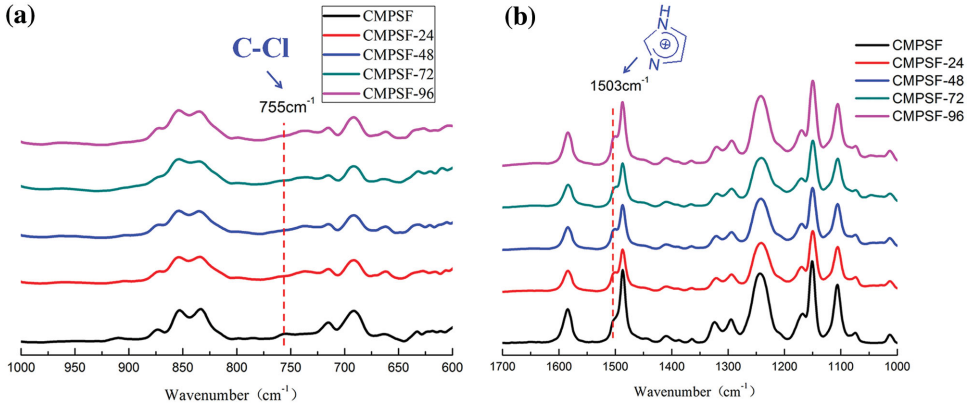

Figure 1. FTIR of charged crosslinked membranes.

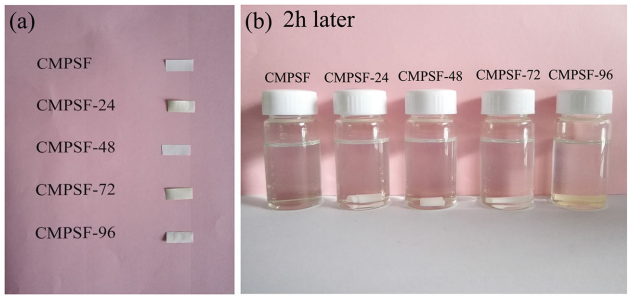

Figure 2. Solvent stability experiments of CMPSF-*X* (*X* = 24, 48, 72, or 96): a) the dried membrane with various cross-linking times; b) CMPSF-*X* (*X* = 24, 48, 72, or 96) in DMAc solution after 2 h.

prepared porous membranes in this paper are expected to perfectly solve this stability problem and provide more options for VFB membrane development.

2. Results and Discussion

In this paper, sponge-like CMPSF membranes were first prepared via the water vapor phase inversion method, which is prone to form highly symmetric, spongy, porous structures and is highly convenient for further upscaling compared with traditional hard template methods.[18] Afterwards, positively charged imidazolium groups were introduced on the pore walls of CMPSF to form an internal crosslinked network. The charge density of the membranes is tuned via controlling the crosslinking time. The prepared charged membranes with different cross-linking time were referred to as CMPSF-*X*, where *X* is the cross-linking time in the imidazole solution. CMPSF-*X* (*X* = 24, 48, 72, or 96) membranes were protonated in 3 mol L^{-1} H_2SO_4 before use.

Figure 1 shows the Fourier transform infrared (FTIR) spectra of CMPSF-*X* (24, 48, 72, or 96). The absorption bands at 755 cm^{-1} correspond to the C—Cl stretch.[19] After crosslinking, the absorption band at about 755 cm^{-1} disappeared, while a new absorption appeared at 1503 cm^{-1}, which is attributed to the stretching of imidazolium.[19] The results indicated that the charged imidazolium groups had been successfully introduced in the porous CMPSF membranes.

To further confirm the crosslinking structure, solvent stability experiments were carried out on pristine and crosslinked porous CMPSF membranes by immersing the membranes in DMAC (**Figure 2**). It can be seen that the pristine CMPSF was completely dissolved in DMAc after 34 min, while no changes were observed for a cross-linked CMPSF-*X* (*X* = 24, 48, 72, or 96) membrane. The results thus indicated that the expected imidazolium crosslinking structure was formed successfully.

Figure 3 showed scanning electron microscope (SEM) images of cross-section and surface morphologies of CMPSF and CMPSF-72. As shown in Figure 3a,e, the cross-sections of CMPSF and CMPSF-72 possessed similar a symmetrical, sponge-like, porous structure, indicating that the membrane morphology hardly changed during crosslinking. The magnified cross-section of CMPSF and CMPSF-72 (Figure 3b,f) indicates that the internal, closed porous structures were integrally maintained after crosslinking. The thickness of the prepared membranes was about 45 ± 5 µm. As shown in Figure 3c,d and g,h, also the surface morphology of CMPSF and CMPSF-72 indicates hardly any changes after cross-linking.

High angle annular dark field scanning transmission electron microscopy (HAADF-STEM) was carried out on CMPSF-24 and CMPSF-72 membranes after $[PdCl_4]^{2-}$ staining to investigate the distribution of the positively charged imidazolium groups on super-thin pore walls.[14] As shown in **Figure 4**, Pd nanoparticles were clearly found surrounding the pores, due to the interaction between the negatively charged $[PdCl_4]^{2-}$ and the positively charged imidazolium groups, suggesting that the imidazolium groups were successfully introduced on the pore walls of the CMFSF membranes. Compared with CMPSF-24, the CMPSF-72 exhibited a more symmetrical distribution of nanoparticles with much higher density, suggesting a higher

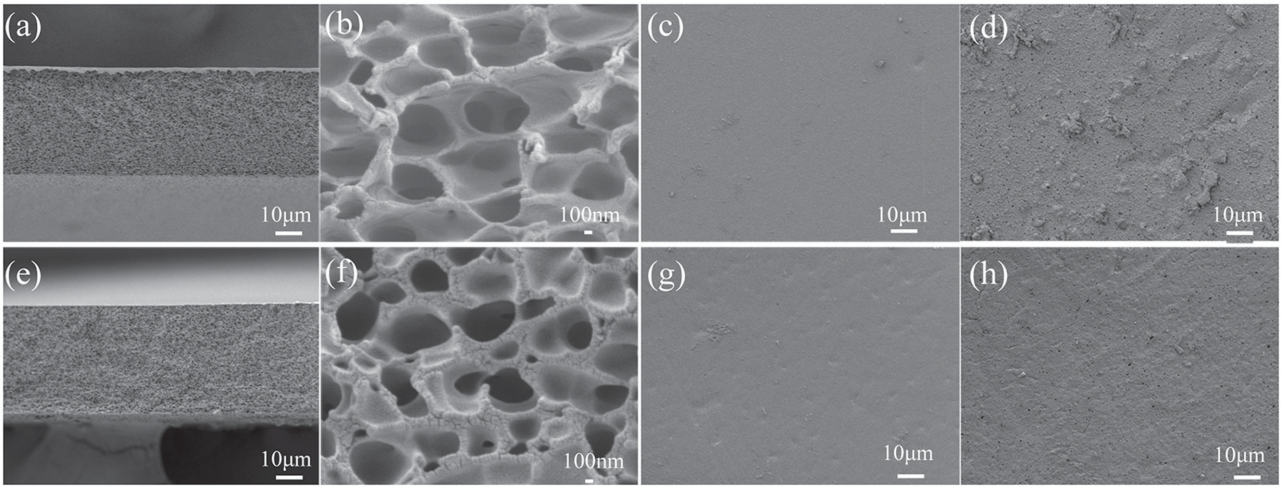

Figure 3. SEM images of cross-section and surface morphology of a–d) CMPSF and e–h) CMPSF-72: a,e) Cross-section and b,f) magnified cross-sectional images of CMPSF and CMPSF-72; c,d,g,h) Surface morphology of CMPSF and CMPSF-72; c,g) surface morphology upon glass side of CMPSF and CMPSF-72; d,h) surface morphology upon vapor side of CMPSF and CMPSF-72.

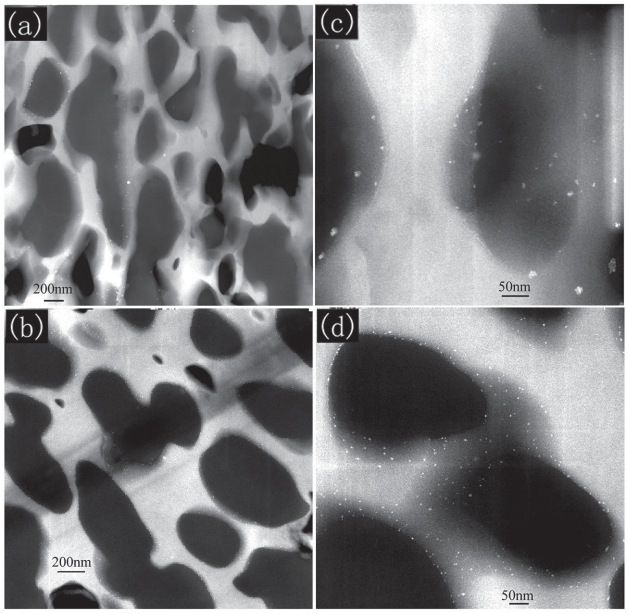

Figure 4. STEM images of a) CMPSF-24 and b) CMPSF-72 stained with $[PdCl_4]^{2-}$; Magnified images of c) CMPSF-24 and d) CMPSF-72.

amount of imdazolium groups with longer crosslinking time (Figure 4d).

The thermal stability of prepared membranes was investigated by thermogravimetric analysis (TGA) (**Figure 5**). The weight loss at around 310 °C in the curve of pristine CMPSF membrane is attributed to the decomposition of C—Cl,[20] while weight loss at around 450 °C is due to the main chain decomposition.[20] For the crosslinked CMPSF, a weight loss was clearly found in the temperature range from 220 °C to 240 °C, which corresponds to the thermal decomposition of the crosslinked imidazolium structure.

The physicochemical properties of CMPSF-*X* (*X* = 24, 48, 72, or 96), including contact angle, swelling and IEC, are shown in **Table 1**. With increasing crosslinking degree, the CMPSF-X membranes become more hydrophilic and the contact angle gradually decreases due to the higher content of hydrophilic imidozalium groups. The IEC of the membranes increased from 1.36 to 1.56 meq g^{-1}, when increasing the crosslinking time from 24 to 96 h, while swelling of the prepared

Table 1. The physicochemical property of CMPSF-*X* (*X* = 24, 48, 72, or 96).

Code	Contact angle [°]	Swelling [%]	Area resistivity [Ω cm^2]	IEC [meq g^{-1}]	Porosity [%]
CMPSF	90.5	0.20	—	—	—
CMPSF-24	64.5	3.22	1.91	1.36	72.1
CMPSF-48	59.5	3.41	1.43	1.44	72.2
CMPSF-72	55.0	3.28	1.22	1.51	72.1
CMPSF-96	53.0	3.38	1.16	1.56	71.9

membranes did not change significantly. This is possibly due to the combined effects of cross-linking and increased hydrophilicity from imidozolium groups: with higher contents of hydrophilic imidozalium groups, more water is expected to be absorbed, while the increased crosslinking degree derived from the high content of imidozalium groups will suppress the swelling.

The area resistance of CMPSF-*X* (*X* = 24, 48, 72, or 96) membranes was reduced from 1.91 to 1.16 Ω cm^2, with crosslinking time increasing from 24 to 96 h due to the increased number of imidazolium groups, showing very good ion conductivity. The results are possibly attributed to the special ion transport mechanism of designed membrane structure, where the ion transport is affected by both the Grotthuss mechanism realized by the imidazolium groups and the diffusion mechanism linked to the porous structure.[21] Apart from ion diffusion, the channels formed by the imidazolium groups can be beneficial for the ion transportation as well.

The permeability of CMPSF-72 and Nafion 115 for vanadium ions is described in **Figure 6**. As shown in Figure 6b, no obvious color change can be observed in the right cell when employing CMPSF-72 as membranes, even after 20 d, while a serious crossover can be found when using Nafion 115 as a membrane, thus demonstrating the excellent selectivity of prepared membranes. The slope of the line related to Nafion 115 in Figure 6a is clearly much higher than that of CMPSF-72, hence further confirming that CMPSF-72 possessed a much higher selectivity than Nafion 115. These results are possible thanks to the Donnan exclusion realized by the positively charged imidazolium groups.

Combing the high selectivity and conductivity, an outstanding VFB performance for energy conversion is expected

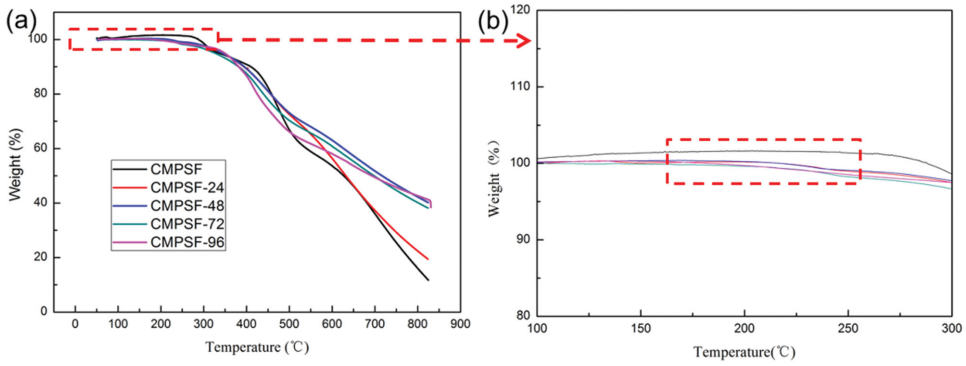

Figure 5. a) Thermogravimetric analysis (TGA) of CMPSF with various crosslinking times; b) locally enlarged details in the range from 220 °C to 240 °C.

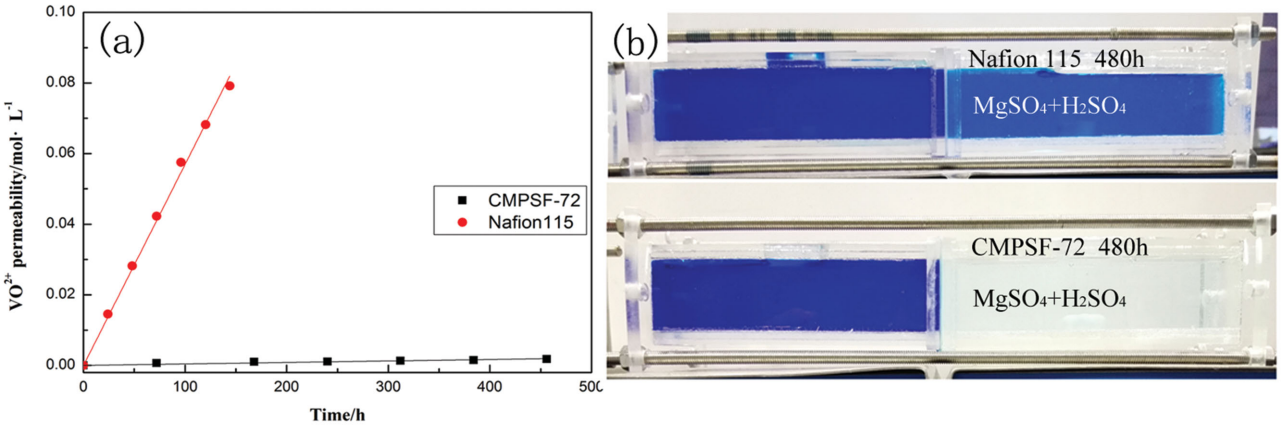

Figure 6. VO^{2+} permeability though Nafion 115 and CMPSF-72.

when using these membranes. The performance of single cells assembled with CMPSF-*X* (*X* = 24, 48, 72, or 96) membranes at a current density of 80 mA cm^{-2} is shown in **Figure 7**. The CE of all above reported membranes stayed above 99%, indicating the excellent selectivity of the prepared membranes. The VE, which is a ratio of a single cell's mean discharge voltage divided by its mean charge voltage, of CMPSF membranes with different cross-linking time improved from 81.5% to 86.6% with a cross-linking time increasing from 24 to 96 h due to the increased conductivity. After 72 h, the VE remains constant, indicating that the equilibrium of the crosslinking reaction is reached at that time. The energy efficiency (EE), which is a very important parameter reflecting the energy conversion ratio, increased from 80.7% to 85.4% when applying membranes with increasing crosslinking time. A VFB assembled with a CMPSF-72 showed an optimized CE of 99.4% and an EE of 86.0%, which is much higher than when using Nafion 115 (93.5%; 82.3%).

The performance of a single cell assembled with a CMPSF-72 at current densities ranging from 40 to 160 mA cm^{-2} is shown in **Figure 8**. The CE remained above 99%, indicating an outstanding selectivity under various current densities. The VE declined with increasing current densities because of the higher ohmic polarization and overpotential.[17] As a consequence, this membrane exhibited a CE of 99.2% and an EE of 80.8% at a current density of 120 mA cm^{-2}.

The temperature-dependent behavior of prepared membranes was evaluated in a charge/discharge test from −5 °C to 50 °C (**Figure 9**). At lower temperatures, the electrolyte becomes more viscous and the proton and vanadium ion transportation becomes restricted. The VE of the battery decreases accordingly. For Nafion 115, with increasing temperature, a decreased CE and an increased VE were observed, due to the combined effects of increased vanadium ion crossover, improved electrode kinetics and decreased ohmic polarization of the battery.[22] Compared with Nafion 115, the CE of prepared porous membranes changed only slightly with increasing temperature (all values above 99%), due to the extremely high selectivity. Therefore, a single cell assembled with the CMPSF-72 membrane showed a much higher EE than with a Nafion115 at temperatures above 15 °C.

This is possibly due to that the sulfonated groups in Nafion could aggregate into hydrophilic clusters, which can provide a much larger cation transport channel, leading to higher proton conductivity as well as low selectivity. At relatively higher temperature, the low selectivity could induce much

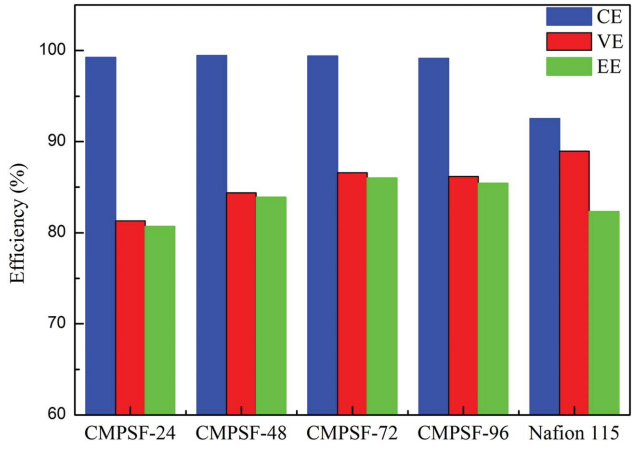

Figure 7. VFB performance of Nafion 115 and CMPSF-*X* (*X* = 24, 48, 72, or 96) at 80 mA cm^{-2}.

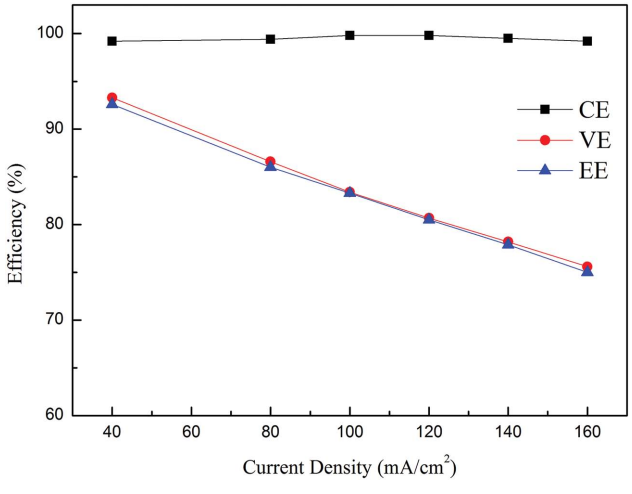

Figure 8. VFB performance of CMPSF-*X* (*X* = 24, 48, 72, or 96) at different current densities.

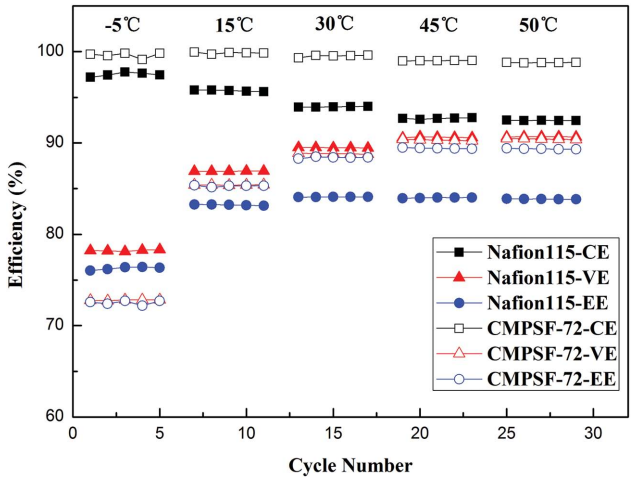

Figure 9. VFB performance of CMPSF-*X* and Nafion 115 at various temperatures.

lower CE of Nafion and further lower EE. However, at lower temperature, more viscous electrolytes will lead to much lower transfer rate of protons, the voltage efficiency will decrease. Compare with CMPSF-72, the voltage efficiency of Nafion 115 will decrease much slighter than the CMPSF-72, since Nafion possesses much larger ion transport channel and further result in higher EE.

To investigate the chemical stability of the prepared porous membranes under strong acidic and oxidizing conditions, a VFB assembled with a CMPSF-72 was cycled at a current density of 120 mA cm^{-2} (**Figure 10**). The battery showed a stable VFB performance after running continuously for more than 6000 cycles. The surface and cross-section morphologies of CMPSF-72 membranes rarely changed (Figure S3, Supporting Information) after 6000 charge–discharge cycles, suggesting the excellent stability of prepared membranes. In addition, an ex situ stability experiment has been carried out on CMPSF-72, confirming the excellent stability as well. (Figure S4, Supporting Information).

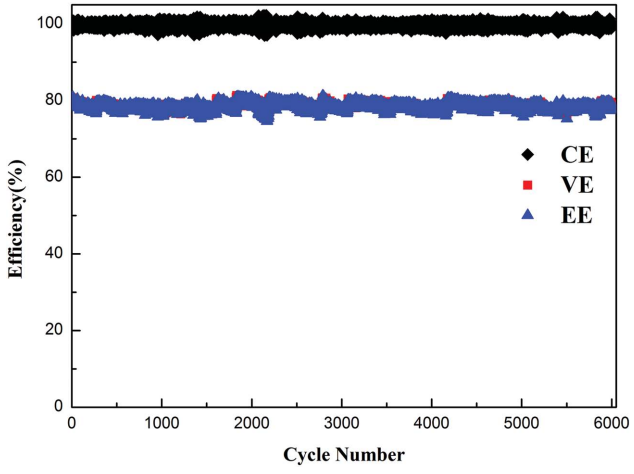

Figure 10. Cycle performance of CMPSF-72.

This unprecedented high stability of the VFB system applying the prepared membranes is attributed to the cross-linked structure, which restricts swelling and further declines the VO_2^+ oxidization. This excellent cycle performance of CMPSF-72 is the first reported porous membranes to meet the long-term chemical stability requirements under the harsh environment of a VFB.

The characteristics of capacity retention and transfer behavior are of important properties for VFB.[23,24] **Figure 11** illustrates the change of volume and molar quantity vanadium ions at the positive and negative side upon cycling when employing CMPSF-72 and Nafion 115 as a membrane. For Nafion 115, the electrolyte volume increased notably in the positive half-cell and decreased in the negative half-cell as cycle proceeded. This tendency is more obvious during the first 20 cycles after which the electrolyte volume in the positive and negative half-cells changed slightly. While for CMPSF-72, the electrolyte volume in the positive half-cell initially increased and then decreased. Compared with Nafion 115, the prepared CMPSF-72 shows a much slower transfer rate of vanadium ions, further leading to much less imbalance. The change of total vanadium ions with different valences during the cycling test is shown in Figure 11b–d. When employing Nafion 115 as a membrane (Figure 11b), the molar quantity of vanadium ions slowly increased on the positive side and decreased on the negative side at the end of the discharge, while for CMPSF-72, the total amount of vanadium ions in the positive and the negative half-cell had changed only very slightly by the end of the discharge process.[24] At the end of the discharge process in Figure 11c,d, a large amount of VO^{2+} at the positive electrolyte side was accumulated and the amount of V^{3+} at the negative electrolyte side was consumed when employing Nafion 115 as a membrane, while concentrations of the various vanadium ions hardly changed in each half-cell for CMPSF-72, demonstrating the very high selectivity of prepared membranes.

As described above, the transfer of vanadium ions will inevitably lead to some capacity loss as cycling proceeds. The discharged capacity as cycling, when using Nafion 115 and CMPSF-72 as membranes, is indicated in **Figure 12**. CMPSF-72 showed a much higher capacity retention than Nafion 115, which was in accordance with the results of the transfer behavior of the various ions. Compared with Nafion 115, CMPSF-72 showed a much lower ion transfer rate, which would lead to less discharge during the cycle process and to a higher retention of capacity. Such capacity retention is essential to allow a VFB system to consistent produce energy with minimal system maintenance.

3. Conclusion

Advanced charged sponge-like membranes with an internal crosslinked network covering the pore walls were successfully fabricated and utilized in VFB applications. The introduction of positively charged imidazolium groups on the pore walls of the membranes effectively restricted the vanadium transport across the membrane and improved the ionic conductivity. As a result, the VFB performance of a single cell assembled with CMPSF-72 exhibited a CE above 99% and an EE of about 86%

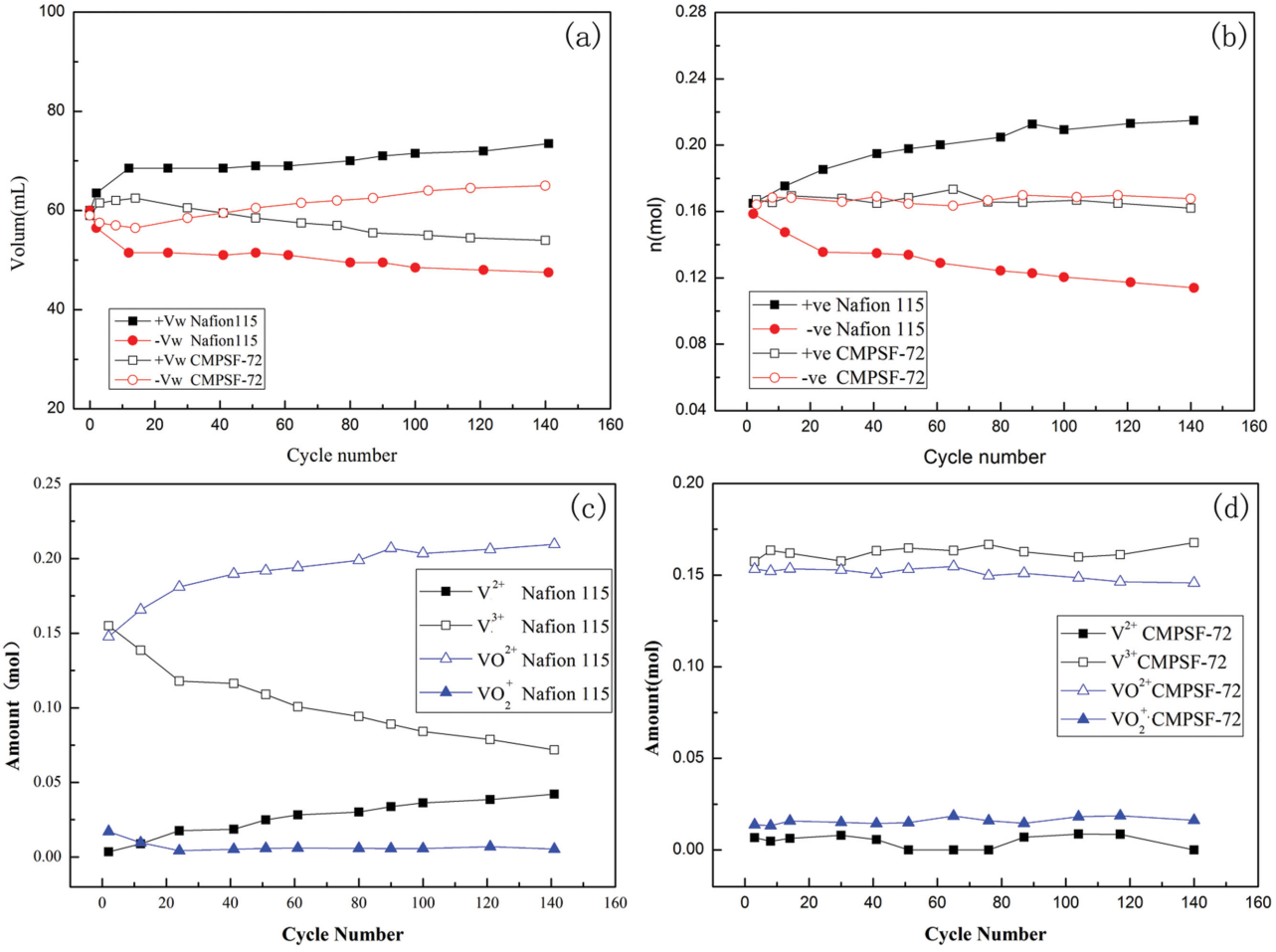

Figure 11. a) Electrolyte volume change in the positive and negative half-cell with Nafion 115 and CMPSF-72 and ion-transfer behavior for Nafion 115 or CMPSF-72 as membranes: b) change of total amount of vanadium ions in positive and negative half-cell; c) vanadium ions with various valences for Nafion 115; d) vanadium ions with various valences for CMPSF-72.

at a current density of 80 mA cm^{-2}. Moreover, a VFB assembled with these membranes showed a stable performance over more than 6000 charge/discharge cycles, which is up to now the longest cycle life ever reported, proving excellent membrane stability. The developed porous membrane thus provides a powerful substitute for Nafion 115 to further promote commercialization of VFB.

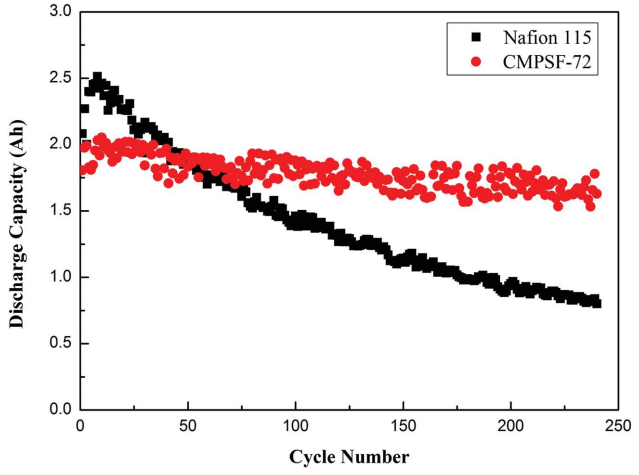

Figure 12. Discharged capacity retention during a cycle process using Nafion 115 and CMPSF-72 as membrane.

4. Experimental Section

CMPSF Membrane Preparation: The CMPSF porous membranes were prepared via the water-vapor-induced phase inversion method. CMPSF (the synthetic details were reported in Supporting Information) was first dissolved in dimethylacetamide (DMAc) to form a 20 wt% solution. The solution was cast on a clean, dust-free glass plate, which was then transferred to a constant climate chamber (BPS-100CL, Hangzhou Haxi), (50 °C and 100% humidity) for 10 min to form a spongy structure. Afterward, the membranes were peeled off and soaked in deionized water before crosslinking.

Membrane Crosslinking: Membranes with fixed size of 11.4 × 9.0 cm^2, were immersed in a 300 mL 10 wt% imidazole solution in water at 60 °C for different times. Afterward, the membranes were washed with and stored in deionized water for use.

Attenuated Total Reflection Flourier Transformed Infrared Spectroscopy: The chemical structure of the membranes was characterized using a JASCO FTIR 4100 spectrometer. Each spectrum was recorded at a rate

of 48 scans with a resolution of 4 cm^{-1}, collected from 600 to 4000 cm^{-1} in absorption mode.

High Angle Annular Dark Field Scanning Transmission Electron Microscopy: HAADF-STEM images were recorded on a FEIF30 microscope with a resolution of 0.17 nm operated at an acceleration voltage of 300 kV. The samples were first treated with a 0.02 mol L^{-1} palladium chloride solution and fixed in epoxy, before being cut into thin slice samples.

Scanning Electron Microscope and Field Emission Scanning Electron Microscope: The cross-sections and surface morphologies of membranes were recorded by SEM (JEOL 6360LV, Japan) and FE-SEM (QUANTA 200FEG), respectively. The samples were obtained by breaking them in liquid nitrogen. All samples were gold coated before use.

Contact Angle: Hydrophilicity of the membranes was investigated by contact angle measurement (JC2001A, China). 5 µL deionized water was dropped on the flat surface of a dried membrane and the images were frozen after 15 s for all the samples.

Area Resistance: The area resistance of a membrane was measured via a conductivity cell as reported.[6] The cell was filled with 0.5 mol L^{-1} H_2SO_4 in each cell, which was separated by a membrane with an effective area of 1 cm^2. The area resistance was measured by using electrochemical impedance spectroscopy (EIS) over a frequency range from 1 kHz to 1 MHz. The membrane was pretreated in a 0.5 mol L^{-1} H_2SO_4 solution for 24 h. The area resistance (r) is calculated by the formula below:

$$r = A \times (r_1 - r_2) \tag{1}$$

where r_1 and r_2 are the electronic resistance of a conductive cell with and without membrane, respectively, and A is the effective area of a membrane.

Thermogravimetric Analysis: Thermal stability of a membrane was determined by TGA using a TG-DTA analyzer (Perkin Elmer) under N_2 flow, with a heating rate of 5 °C min^{-1}.

Ion-Exchange Capacity: The IECs of prepared membranes were measured via titration.[17] First, the prepared membranes were immersed in a 1 mol L^{-1} NaCl solution for 24 h to convert the ion-exchange groups into Cl^-; then these membranes were rinsed with and immersed in deionized water to remove the redundant Cl^-. Finally, the above prepared membranes were immersed into a 50 mL 1 mol L^{-1} $NaNO_3$ solution to bring the Cl^- into solution. The solution was then titrated by 0.01 mol L^{-1} $AgNO_3$ using K_2CrO_4 as indicator. The IEC was calculated by

$$\mathrm{IEC} = \frac{\Delta V_{\mathrm{AgNO_3}} c_{\mathrm{AgNO_3}}}{m_{\mathrm{d}}} \tag{2}$$

where ΔV_{AgNO_3} is the volume of $AgNO_3$ solution; C_{AgNO_3} is the concentration of $AgNO_3$ and m_d is the mass of dried membrane-X (X = 24, 48, 72 or 96).

Porosity: A CMPSF-X (X = 24, 48, 72, or 96) membrane was immersed into deionized water for 24 h. The surface water on membrane was then quickly wiped out and weighed (M_w). The membrane was subsequently fully dried and weighed (M_d). The porosity of prepared membrane was calculated by

$$P = \frac{(M_{\mathrm{W}} - M_{\mathrm{d}})}{\rho_{\mathrm{water}} V} \times 100\% \tag{3}$$

where M_w is the mass of wet membrane; M_d is the mass of dried membrane; ρ is the density of water at room temperature; V is the volume of dried membrane.

Vanadium Permeability: The selectivity of a membrane was evaluated by vanadium ion permeability. A membrane was assembled in a diffusion cell and a 120 mL 1.5 mol L^{-1} $VOSO_4$ in 3 mol L^{-1} H_2SO_4 solution and a 120 mL 1.5 mol L^{-1} $MgSO_4$ in 3 mol L^{-1} H_2SO_4 solution were filled in the left and right compartments, respectively. The solutions in both chambers were vigorously stirred to minimize concentration polarization. Samples of a 4 mL from the right cell were collected at a regular time interval, then the same volume of original solution was added to the right compartment. The concentration of $VOSO_4$ was measured with a UV-vis spectrometer (JASCO, FT-IR 4100, Japan).

VFB Single-Cell Performance: Similar to our previous report,[17] a VFB single cell was assembled by sandwiching a membrane between two carbon felt electrodes (Liaoyang J-Carbon Materials Co., Ltd., China with thickness of 5 millimeters), clamped by two polar plates. All these components were fixed between two stainless plates. The effective area of an electrode is 48 cm^2 .1.5 mol L^{-1} V^{2+}/V^{3+} in 3 mol L^{-1} H_2SO_4 solutions and a 1.5 mol L^{-1} VO^{2+}/VO_2^+ in 3 mol L^{-1} H_2SO_4 solutions were used as catholyte and anolyte, respectively. The electrolytes were cyclically pumped into the corresponding half-cell. The flow rate of electrolyte is kept at 50–60 mL min^{-1}. The battery performance test was conducted by Arbin BT 2000 at a constant current density ranging from 40 mA cm^{-2} to 160 mA cm^{-2}. The charge–discharge limit voltages were set as 1 and 1.55 V, respectively, to minimize corrosion of carbon felt electrodes and graphite polar plates. All the efficiency data were based on three parallel experiments. The deviation of battery efficiency experiment was less than 2%.

The various vanadium ions and water transfer behavior were investigated during the cycling test. The volume of negative and positive electrolytes was kept at 100 mL. A battery assembled with a membrane (area 48 cm^2) was cycled at a current density of 120 mA cm^{-2}. The volume change of positive and negative half-cells was measured after discharge of each cycle. The vanadium concentration of positive and negative electrolytes was detected using a potentiometric titration method.

Stability Test: To investigate the chemical stability of CMPSF-X porous membrane under the strong acidic and oxidizing condition, the VFB assembled with CMPSF-72 was cycled at a current density of 120 mA cm^{-2}.

Supporting Information

Supporting Information is available from the Wiley Online Library or from the author.

Acknowledgements

X.L. acknowledges the financial support from China Natural Science Foundation (Grant Nos. 21206158, 21476224, and 51361135701) and the Outstanding Youngest Scientist Foundation, Chinese Academy of Sciences (CAS), Key Research Program of the Chinese Academy of Science (KG2D-EW-602-2), and Dalian Municipal Outstanding Young Talent Foundation (2014J11JH131). I.F.J.V. is grateful to KU Leuven for support in the frame of OT (11/ 061) and IDO 12/006, and the Flemish Government for the Methusalem (CASAS) funding and the Federal Government for an IAP grant (FS2).

Received: August 12, 2015
Revised: September 16, 2015
Published online: November 20, 2015

[1] a) J. Liu, J.-G. Zhang, Z. Yang, J. P. Lemmon, C. Imhoff, G. L. Graff, L. Li, J. Hu, C. Wang, J. Xiao, G. Xia, V. V. Viswanathan, S. Baskaran, V. Sprenkle, X. Li, Y. Shao, B. Schwenzer, *Adv. Funct. Mater.* **2013**, *23*, 929; b) B. Dunn, H. Kamath, J.-M. Tarascon, *Science* **2011**, *334*, 928; c) Z. Yang, J. Zhang, M. C. Kintner-Meyer, X. Lu, D. Choi, J. P. Lemmon, J. Liu, *Chem. Rev.* **2011**, *111*, 3577.

[2] M. Skyllas-Kazacos, M. H. Chakrabarti, S. A. Hajimolana, F. S. Mjalli, M. Saleem, *J. Electrochem. Soc.* **2011**, *158*, R55.

[3] G. L. Soloveichik, *Nature* **2014**, *505*, 163.

[4] W. Wang, Q. Luo, B. Li, X. Wei, L. Li, Z. Yang, *Adv. Funct. Mater.* **2013**, *23*, 970.
[5] B. Schwenzer, J. Zhang, S. Kim, L. Li, J. Liu, Z. Yang, *ChemSusChem* **2011**, *4*, 1388.
[6] A. Parasuraman, T. M. Lim, C. Menictas, M. Skyllas-Kazacos, *Electrochim. Acta* **2013**, *101*, 27.
[7] X. Li, H. Zhang, Z. Mai, H. Zhang, I. Vankelecom, *Energy Environ. Sci.* **2011**, *4*, 1147.
[8] a) X. Luo, Z. Lu, J. Xi, Z. Wu, W. Zhu, L. Chen, X. Qiu, *J. Phys. Chem. B* **2005**, *109*, 20310; b) Z. Mai, H. Zhang, X. Li, C. Bi, H. Dai, *J. Power Sources* **2011**, *196*, 482; c) S. Winardi, S. C. Raghu, M. O. Oo, Q. Yan, N. Wai, T. M. Lim, M. Skyllas-Kazacos, *J. Membr. Sci.* **2014**, *450*, 313; d) X. L. Zhou, T. S. Zhao, L. An, L. Wei, C. Zhang, *Electrochim. Acta* **2015**, *153*, 492; e) J. Li, Y. Zhang, S. Zhang, X. Huang, L. Wang, *Polym. Adv. Technol.* **2014**, *25*, 1610.
[9] Z. Yuan, X. Li, J. Hu, W. Xu, J. Cao, H. Zhang, *Phys. Chem. Chem. Phys.* **2014**, *16*, 19841.
[10] H. Zhang, H. Zhang, X. Li, Z. Mai, J. Zhang, *Energy Environ. Sci.* **2011**, *4*, 1676.
[11] H. Zhang, H. Zhang, X. Li, Z. Mai, W. Wei, *Energy Environ. Sci.* **2012**, *5*, 6299.
[12] a) J. Cao, H. Zhang, W. Xu, X. Li, *J. Power Sources* **2014**, *249*, 84; b) W. Wei, H. Zhang, X. Li, H. Zhang, Y. Li, I. Vankelecom, *Phys. Chem. Chem. Phys.* **2013**, *15*, 1766.
[13] a) Y. Li, X. Li, J. Cao, W. Xu, H. Zhang, *Chem. Commun.* **2014**, *50*, 4596; b) Y. Li, H. Zhang, H. Zhang, J. Cao, W. Xu, X. Li, *J. Membr. Sci.* **2014**, *454*, 478.
[14] H. Zhang, H. Zhang, F. Zhang, X. Li, Y. Li, I. Vankelecom, *Energy Environ. Sci.* **2013**, *6*, 776.
[15] a) G.-J. Hwang, H. Ohya, *J. Membr. Sci.* **1997**, *132*, 55; b) Q. Li, C. Pan, J. O. Jensen, P. Noyé, N. J. Bjerrum, *Chem. Mater.* **2007**, *19*, 350.
[16] F. Zhang, H. Zhang, C. Qu, *ChemSusChem* **2013**, *6*, 2290.
[17] W. Xu, Y. Zhao, Z. Yuan, X. Li, H. Zhang, I. F. J. Vankelecom, *Adv. Funct. Mater.* **2015**, *25*, 2583.
[18] Y. Wang, S. Wang, M. Xiao, D. Han, Y. Meng, *Int. J. Hydrogen Energy* **2014**, *39*, 16088.
[19] F. Zhang, H. Zhang, C. Qu, *J. Mater. Chem.* **2011**, *21*, 12744.
[20] J. Zhou, M. Unlu, J. A. Vega, P. A. Kohl, *J. Power Sources* **2009**, *190*, 285.
[21] G. Merle, M. Wessling, K. Nijmeijer, *J. Membr. Sci.* **2011**, *377*, 1.
[22] X. Wei, Z. Nie, Q. Luo, B. Li, B. Chen, K. Simmons, V. Sprenkle, W. Wang, *Adv. Energy Mater.* **2013**, *3*, 1215.
[23] a) T. Sukkar, M. Skyllas-Kazacos, *J. Membr. Sci.* **2003**, *222*, 235; b) A. Tang, J. Bao, M. Skyllas-Kazacos, *J. Power Sources* **2011**, *196*, 10737.
[24] J. Sun, X. Li, X. Xi, Q. Lai, T. Liu, H. Zhang, *J. Power Sources* **2014**, *271*, 1.